Published in final edited form as:
Mol Cell Neurosci. 2014 July ; 0: 241–254. doi:10.1016/j.mcn.2014.07.005.

Postsynaptic actin regulates active zone spacing and glutamate receptor apposition at the *Drosophila* neuromuscular junction

Aline D. Blunk[1], **Yulia Akbergenova**[1], **Richard W. Cho**[1], **Jihye Lee**[1,2], **Uwe Walldorf**[3], **Ke Xu**[4], **Guisheng Zhong**[4], **Xiaowei Zhuang**[4,5], and **J. Troy Littleton**[1]

[1]The Picower Institute for Learning and Memory Department of Biology and Department of Brain and Cognitive Sciences Massachusetts Institute of Technology, Cambridge, MA 02139

[2] The Department of Oral Pathology School of Dentistry, Pusan National University, Korea

[3]Department of Developmental Biology University of Saarland, Homburg/Saar, Germany

[4]Howard Hughes Medical Institute (HHMI) Department of Chemistry and Chemical Biology, Harvard University Cambridge, MA 02138

[5]Department of Physics, Harvard University, Cambridge, MA 02138

Abstract

Synaptic communication requires precise alignment of presynaptic active zones with postsynaptic receptors to enable rapid and efficient neurotransmitter release. How transsynaptic signaling between connected partners organizes this synaptic apparatus is poorly understood. To further define the mechanisms that mediate synapse assembly, we carried out a chemical mutagenesis screen in *Drosophila* to identify mutants defective in the alignment of active zones with postsynaptic glutamate receptor fields at the larval neuromuscular junction. From this screen we identified a mutation in actin 57B that disrupted synaptic morphology and presynaptic active zone organization. Actin 57B, one of six *actin* genes in *Drosophila*, is expressed within the postsynaptic bodywall musculature. The isolated allele, act^{E84K}, harbors a point mutation in a highly conserved glutamate residue in subdomain 1 that binds members of the Calponin Homology protein family, including spectrin. Homozygous act^{E84K} mutants show impaired alignment and spacing of presynaptic active zones, as well as defects in apposition of active zones to postsynaptic glutamate receptor fields. act^{E84K} mutants have disrupted postsynaptic actin networks surrounding presynaptic boutons, with the formation of aberrant actin swirls previously observed following disruption of postsynaptic spectrin. Consistent with a disruption of the postsynaptic actin cytoskeleton, spectrin, adducin and the PSD-95 homolog Disc-Large are all mislocalized in act^{E84K} mutants. Genetic interactions between act^{E84K} and *neurexin* mutants suggest that the postsynaptic actin cytoskeleton may function together with the Neurexin-Neuroligin transsynaptic

*Correspondence to: J. Troy Littleton Massachusetts Institute of Technology 43 Vassar Street, 46-3243 Cambridge MA 02139 (O) 617-452-2605 (Fax) 617-452-2249 troy@mit.edu.

signaling complex to mediate normal synapse development and presynaptic active zone organization.

Keywords

Actin; Synapse; Spectrin; NMJ; Cytoskeleton; Neurexin

INTRODUCTION

The presynaptic active zone (AZ) organizes the synaptic release machinery to facilitate neuronal communication (reviewed in Südhof, 2013). The AZ is composed of an electron-dense cytomatrix enriched with specialized proteins that serve as a scaffold for the synaptic vesicle trafficking machinery (Sigrist and Schmitz, 2011). The organization of AZs, including their spacing, density and alignment with postsynaptic receptor fields, is tightly regulated to ensure efficient synaptic transmission. AZ density at neuromuscular junctions (NMJs) remains constant throughout development (Meinertzhagen et al., 1998; Clarke et al., 2012; Nishimune, 2012), indicating tight control over AZ assembly. Transsynaptic cell adhesion complexes are thought to mediate coordinated assembly of pre- and postsynaptic specializations (Dalva et al., 2007; Giagtzoglou et al., 2009; Sun and Xie, 2012), although the signaling pathways underlying AZ organization are largely unknown.

The *Drosophila* NMJ serves as a model synapse for identifying regulators of AZ biology. Previous genetic screens have revealed several signaling pathways that modulate AZ assembly (Sigrist and Schmitz, 2011). A diverse set of proteins have been identified in these screens, ranging from the endocytosis regulator synaptojanin (Dickman et al., 2006), the synaptic vesicle associated GTPase Rab3 (Graf et al., 2009), the serine threonine kinase Unc-51 (Wairkar et al., 2009) to the postsynaptic spectrin cytoskeleton (Pielage et al., 2006). In addition, proper alignment of the AZ with postsynaptic receptors requires transsynaptic communication provided by the Neurexin-Neuroligin and Teneurin synaptic cell adhesion proteins (Li et al., 2007; Banovic et al., 2010; Mosca et al., 2012).

To identify additional pathways that control synapse organization, we carried out a chemical mutagenesis screen in *Drosophila*. Using fluorescently-conjugated antibodies against the presynaptic AZ protein Bruchpilot (BRP) (Wagh et al., 2006) and the postsynaptic glutamate receptor subunit III (GluRIII) (Marrus, 2004), we screened for mutants that disrupted AZ size, number, location or apposition to postsynaptic glutamate receptors. From the screen we identified a mutation in actin 57B, one of six *actin* genes in *Drosophila* and the main isoform present in postsynaptic muscles (Fyrberg et al., 1980; Tobin et al., 1980), that disrupted normal AZ organization. Here we describe our characterization of the isolated allele, which results from mutation of glutamate 84 (act^{E84K}) in subdomain 1 of actin, a region required for spectrin binding. We find that postsynaptic actin 57B is a key organizer of AZ assembly, linking several protein networks to ensure coordinated pre- and postsynaptic maturation. Postsynaptic F-actin structure is severely disrupted in act^{E84K} mutants, with abnormal actin swirls replacing the typical uniform structure of the actin-rich postsynaptic domain. In addition, the structure of the postsynaptic density is perturbed, with

defects in subsynaptic reticulum (SSR) formation and mislocalization of Discs-Large, spectrin and adducin. The disruption of the postsynaptic cytoskeleton leads to a reduction in AZ density and an increase in unapposed AZs and glutamate receptor clusters. These findings indicate that synaptic interactions altered in act^{E84K} mutants perturb postsynaptic cytoskeletal structure and disrupt transsynaptic signals required for presynaptic AZ organization.

RESULTS

EMS mutagenesis screen for regulators of synaptic growth and organization

The *Drosophila* NMJ provides a powerful model system to characterize synaptic organization. During its life cycle, *Drosophila* undergoes 3 larval stages marked by a significant increase in muscle size. To ensure efficient muscle contraction, the NMJ arbor expands ~10 fold during development, adding new synaptic boutons and increasing the number of AZs through an activity-dependent process (Stewart et al., 1996; Zito et al., 1999). To identify regulators of AZ organization and synapse formation, we carried out an unbiased EMS mutagenesis screen of the 2nd chromosome. Immunostaining with antibodies against the AZ component Bruchpilot (BRP) (Wagh et al., 2006) and the essential Glutamate receptor subunit III (DGluRIII) (Marrus, 2004) shows a regular grid-like spatial organization of AZs at 3rd instar NMJs of control animals (Fig. 1A). This assay also allowed identification of mutations affecting synaptic growth and stability, as BRP and DGluRIII distributions highlighted overall NMJ morphology. Synaptic arbors innervating muscle 4 contain ~10 to 20 AZs per bouton, depending on bouton size. Changes in AZ size, distribution and postsynaptic DGluRIII apposition were easily identified at this synapse. Similar strategies have been previously used to successfully study active zone formation and alignment, as well as synaptic development (Graf et al., 2009; Viquez et al., 2009; Wairkar et al., 2009; Valakh et al., 2012; Enneking et al., 2013). We mutagenized males of an isogenized Canton-S line (hereafter referred to as control) and backcrossed single male progeny to a GFP balancer strain to generate homozygous lines for screening. Among a total of 691 lines screened at the 3rd instar larval stage, 30 mutant strains were identified with abnormal synaptic morphology. These mutants were categorized into several phenotypic classes: aberrant AZ distribution, AZ apposition defects, DGluRIII clustering defects (Fig. 1B), synaptic growth defects (Fig. 1C) and bouton size abnormalities (Fig. 1D). We chose to focus our initial analysis on line 117B, which displayed a profound disorganization in presynaptic AZ number and spacing (see below).

Actin 57B mutants show aberrant active zone spacing and density

During development, the *Drosophila* NMJ undergoes synaptic expansion while maintaining constant AZ density (Meinertzhagen et al., 1998; Reiff et al., 2002; Sigrist et al., 2002). Several regulators of AZ number and distribution have been identified (Dickman et al., 2006; Pielage et al., 2006; Graf et al., 2009; Wairkar et al., 2009). However, the molecular mechanisms that define AZ number, spacing and density remain largely unknown (reviewed in Clarke et al., 2012). In control larvae, BRP puncta show a regular distribution throughout synaptic boutons, and are directly apposed to postsynaptic glutamate receptor fields (Fig. 1A, 2A). One of the AZ mutants identified in our EMS screen, line 117B, exhibited

abnormal spacing and distribution of BRP puncta in presynaptic boutons compared to controls. Instead of the regular spaced array of AZs found in control, some synaptic boutons contained large BRP clusters, whereas others were nearly devoid of BRP puncta (Fig. 2B). Given the severity of the phenotype in this line, we characterized the mutant in more detail. Homozygous 117B larvae displayed reduced locomotion and growth, and rarely survived to pupation. Meiotic recombination mapping of the lethality placed the 117B locus between 2-94 and 2-99. Further refinement with deficiency mapping indicated that the mutation resides at 57B4-B5, defined by the breakpoints of deficiencies *Df(2R)BSC404* and *Df(2R)BSC814*. To confirm the AZ phenotype, in addition to the lethality, mapped to this cytological interval, we performed morphological analysis of 117B in trans to *Df(2R)Exel7166* that deletes the 57B3-57B5 interval. 117B/*Df(2R)Exel7166* larvae showed a similar lethal stage, and immunocytochemical analysis demonstrated profound defects in AZ organization, with some boutons lacking AZs altogether, and other displaying clumping of AZs within the terminal (Fig. 2C, D). Sequence analysis of the 7 candidate genes uncovered by the overlap of the deficiencies revealed a point mutation of the highly conserved residue glutamate 84 to lysine (E84K) in one of the six *Drosophila actin* genes, *actin 57B* (Fyrberg et al., 1980).

We next characterized synaptic morphology phenotypes in the 117B mutant, hereafter referred to as act^{E84K}. Concomitant with the initially observed defect in presynaptic AZ distribution, homozygous act^{E84K} mutants also exhibited changes in the size and localization of glutamate receptor fields. At control NMJs, glutamate receptors clustered into distinct receptor fields directly apposed to presynaptic AZs. DGluRIII cluster shape was abnormal in act^{E84K} mutants, with fused receptor fields often observed opposite large presynaptic BRP clusters (see below). Homozygous act^{E84K} mutants were smaller than age-matched control animals (Fig. 2E) (control: 36640 ± 1542 μm^2 muscle area, n=15; act^{E84K}: 12550 ± 580.9 μm^2 muscle area, n=33; $p<0.0001$). However, total bouton number per muscle area was not significantly different from control (Fig. 2F) (control: 15.19 ± 1.37, n=8; act^{E84K}: 19.56 ± 1.52, n=11; p=0.056). Total AZ number normalized to bouton number revealed a reduction compared to controls (Fig. 2G) (control: 7.54 ± 0.24, n=8; act^{E84K}: 6.165 ± 0.34, n=11; p=0.0071). Bouton volume was slightly increased compared to control, indicating the reduced number of AZs per bouton in act^{E84K} mutants is not due to a reduction in bouton volume (Fig. 2H) (control: 7.47 ± 0.35 μm^3, n=416; act^{E84K}: 8.84 ± 0.49 μm^3, n=273; $p=0.0189$). AZ density has been shown to remain constant at mammalian and *Drosophila* NMJs throughout development (Meinertzhagen et al., 1998; Reiff et al., 2002; Chen et al., 2011; Sigrist and Schmitz, 2011). While control animals have ~one AZ per μm^3, significantly fewer AZs per bouton volume were observed in act^{E84K} (Fig. 2I) (control: 1.12 ± 0.02 AZ/μm^3, n=416; act^{E84K}: 0.76 ± 0.34 AZ/μm^3, n=273; $p<0.0001$). As expected from the regular distribution of BRP at the NMJ of wild-type animals, the frequency distribution displays a peak at one AZ per μm^3 volume in control boutons (Fig. 2J, K). In act^{E84K} mutants, a significant shift towards fewer AZs per bouton volume was observed, indicating a loss of ordered AZ spacing ($p<0.0001$). These findings indicate Actin 57B is a key organizer of NMJ morphology and AZ spacing.

Postsynaptic actin cytoskeleton assembly is impaired in *act^{E84K}*

Actin is a highly conserved protein with few sequence changes across evolution (Fig. 3A). The six *Drosophila actin* genes are highly conserved, differing in only 27 nucleotides. However, they show spatial and temporal specific expression patterns that have been well characterized in *Drosophila* (Fyrberg et al., 1983; Tobin et al., 1990a; Fyrberg et al., 1998). Actin 57B, one of four muscle actins, is the main actin present in larval bodywall muscles that constitute the postsynaptic compartment during our developmental screening window (Fyrberg et al., 1983; Tobin et al., 1990a; Kelly et al., 2002). In contrast, Actin 5C and Actin 42A are ubiquitous isoforms that are also found in the presynaptic compartment (Fyrberg et al., 1983; Burn et al., 1989; Tobin et al., 1990b). As such, we expected the mutation in Actin 57B to disrupt an aspect of actin function in the postsynaptic compartment, given its localization to the muscle during development. Sequencing of the *act^{E84K}* genomic locus revealed a mutation that changed the highly conserved glutamate 84 residue to lysine (E84K) (Fig. 3A). E84 lies in subdomain 1 of the actin monomer, facing out from the actin filament (Fig. 3B-D). This actin region has been implicated in binding to members of the Calponin Homology (CH) domain superfamily, including β-spectrin, α-actinin and dystrophin (Atwood et al., 1993; Honts et al., 1994; McGough et al., 1994; Hanein et al., 1997; Hodgkinson et al., 1997; Petersen et al., 1997; Moores et al., 2000; Galkin, 2002; Sutherland-Smith et al., 2003).

Based on the location of the E84K mutation and its potential to disrupt interactions with other members of the cytoskeleton, we analyzed the organization of the actin-based cytoskeletal network in the postsynaptic muscle. F-actin forms the thin filaments of the sarcomere, which interact with myosin thick filaments and are anchored at the Z-disc. In addition, F-actin is enriched postsynaptically in a halo pattern that surrounds individual synaptic boutons that are embedded just under the surface of the muscle (Coyle et al., 2004; Chen et al., 2005; Nunes et al., 2006; Graf et al., 2009; Ramachandran et al., 2009), forming a key component of the postsynaptic spectrin cytoskeleton at the NMJ (Bennett and Baines, 2001; Dubreuil and Das, 2009; Baines, 2010). The toxin phalloidin selectively binds F-actin and can be used to visualize sarcomeric and NMJ actin. In larval body-wall muscle of control animals, bundled myofibrils and their sarcomeric I-band pattern were evident (Fig. 4A). This structure was preserved in age-matched *act^{E84K}* mutant larvae, indicating the E84K mutation does not disrupt sarcomere and myofibril assembly (Fig. 4B). However, aberrant actin filaments were apparent outside of the sarcomeric organization, concentrating around the NMJ (Fig. 4B). Instead of the normal homogenous distribution of actin surrounding boutons in control animals (Fig. 4C, E), *act^{E84K}* mutants displayed large actin swirls (Fig. 4D, F), similar to the abnormalities seen in β-spectrin mutants (Pielage et al., 2006; Ramachandran et al., 2009). Together with the location of E84 in the CH domain-binding site of actin, we hypothesized that the *act^{E84K}* mutation is likely to disrupt β-spectrin interactions with actin filaments that normally organize the postsynaptic cytoskeleton.

Defects in localization of postsynaptic spectrin cytoskeleton components in *act^{E84K}*

Spectrin was originally identified in erythrocytes and is widely expressed in most cell types, including neurons (Marchesi and Steers, 1968; Tillack et al., 1970; Bennett et al., 1982;

Bennett and Davis, 1983; Bennett and Lambert, 1991; Bennett and Gilligan, 1993). In nonerythrocyte cells, spectrin is not uniformly distributed, but is thought to establish specialized plasma membrane regions (reviewed in Bennett and Gilligan, 1993; Dubreuil and Das, 2009). In axons, spectrin and actin form a highly periodic lattice structure underneath the axonal membrane (Xu et al, 2013). Interaction of α-spectrin and β-spectrin leads to formation of anti-parallel heterodimers. Further association into heterotetramers enables β-spectrin to connect short actin filaments via its N-terminal CH domain, forming a lattice-like protein network at the plasma membrane (reviewed in Baines, 2010). α- and β-spectrin are localized at the *Drosophila* NMJ and are enriched in both pre- and post-synaptic compartments (Featherstone et al., 2001; Pielage et al., 2005; Pielage et al, 2006). Our data, together with the well-established expression pattern of Actin 57B in muscles, suggest that the act^{E84K} mutation may disrupt postsynaptic actin-spectrin interactions. To test this possibility, we performed immunostaining for spectrin in act^{E84K} animals. At control NMJs, α-spectrin was enriched at the postsynaptic SSR surrounding presynaptic boutons (Fig. 5A). In contrast, act^{E84K} homozygous larvae showed a severe redistribution of α-spectrin away from synaptic boutons (Fig. 5B). The organized spectrin halo structure observed in control animals was largely lost, leading to aberrant localization of the spectrin cytoskeleton in act^{E84K} mutants. High-resolution three-dimensional STORM microscopy performed in control and act^{E84K} mutants confirmed a loss of the structured arrangement of α-spectrin molecules that normally form the postsynaptic cytoskeletal halo around boutons (Fig. 5C-D'). These data indicate the actin-spectrin lattice at the muscle plasma membrane is disrupted in act^{E84K} mutants.

Spectrin is recruited to actin filaments by the actin-capping protein adducin (Gardner and Bennett, 1987; Bennett et al., 1988; Kuhlman et al., 1996; Li et al., 1998). *Drosophila* has a single adducin homolog, Hu-li Tai shao (Hts), which localizes both pre- and post-synaptically at the NMJ and regulates synapse stabilization and growth (Yue and Spradling, 1992; Pielage et al., 2011). We examined the localization of adducin in act^{E84K} mutants, and found the protein was mislocalized in act^{E84K} compared to control (Fig. 5E, F). Adducin binds to the sides and barbed ends of actin, and is a known capping protein (Kuhlman et al., 1996; Li et al., 1998). To determine if adducin (*Hts*) and act^{E84K} mutants show similar phenotypes in cytoskeletal organization, we assayed actin distribution in the muscle of *Hts* mutants, which has not been previously characterized. Phalloidin staining of *hts* mutants revealed an actin distribution distinct from act^{E84K} and controls (Fig. 5G and H, vs. Fig. 4D and F). The actin halo surrounding synaptic boutons in the postsynaptic compartment was still present in *hts* mutants. In addition, *hts* mutants displayed abnormal actin rings throughout the muscle (Fig. 5G, H) that were not observed in act^{E84K} mutants or controls (Fig. 4D, F). Given the distinct differences in actin distribution observed in *hts* and act^{E84K}, they are likely to arise through disrupted scaffolding interactions unique to each mutant.

The postsynaptic actin-protein network regulates DLG localization and SSR formation

Similar to vertebrate NMJs, muscle membrane SSR folds surrounding *Drosophila* type I boutons are enriched with neurotransmitter receptors, cell adhesion molecules and scaffolding proteins. Discs-Large (DLG), the *Drosophila* PSD-95 homolog, localizes to the SSR and is crucial for postsynaptic membrane expansion (Lahey et al., 1994; Budnik et al.,

1996). Spectrin and adducin regulate targeting of DLG to the NMJ (Featherstone et al., 2001; Pielage et al., 2006; Wang et al., 2011). The disruption of the spectrin network in act^{E84K} (Fig. 5B, D) suggested potential DLG mislocalization in the mutants. To test this possibility, we analyzed DLG distribution in control and mutant animals. At control NMJs, immunostaining revealed DLG enrichment at the SSR surrounding presynaptic boutons (Fig. 6A). In contrast, this tight DLG localization was disrupted in act^{E84K} mutants, with regions of more diffuse staining, as well as boutons with only a thin layer of DLG accumulation remaining (Fig. 6B). Consistent with altered DLG localization, ultrastructural electron microscopy (EM) analysis of act^{E84K} mutant NMJs revealed a severe disruption of the postsynaptic SSR membrane folds that normally surround presynaptic boutons. EM sections of control NMJs showed numerous membrane folds surrounding each bouton (Fig. 6C), while act^{E84K} boutons showed a smaller SSR with fewer membrane layers and a reduction in thickness (Fig. 6C, D). Occasionally, membrane folds were missing entirely, and regions of presynaptic membrane were seen directly abutting muscle myofibrils in act^{E84K} mutants. Quantification revealed a severe reduction of mean SSR area from 251.2% ± 28.7 of bouton area in control animals (39 boutons from 5 animals) to 68.6% ± 9.4 in mutants (21 boutons from 3 animals; $p<0.0001$) (Fig. 6D). However, AZ length (defined by length of the electron dense area) and synaptic vesicle (SV) size were unchanged (AZ length: control 505.9 ± 21.9 nm, n=58; act^{E84K} 556.6 ± 33.3 nm, n=31; $p=0.19$; SV size: control 35.2 ± 0.64 nm, n=80; act^{E84K} 36.01 ± 0.47 nm, n=80 SV from 5 boutons; $p=0.3386$) (Fig. 6E, F). In summary, our results indicate Actin 57B regulates postsynaptic spectrin cytoskeleton assembly and is required for DLG targeting and subsequent SSR formation.

Organization of the postsynaptic actin network is necessary for active zone alignment

To ensure efficient synaptic transmission, the presynaptic cytomatrix at the AZ (CAZ) must assemble directly opposite postsynaptic neurotransmitter receptor clusters. As the postsynaptic cytoskeleton and AZ spacing is severely disrupted in act^{E84K} mutants, we analyzed how this disruption would impact synapse assembly and function. Immunohistochemical analysis using antibodies against BRP and the DGluRIII subunit revealed defects in proper AZ alignment in act^{E84K} mutants. AZs unapposed to postsynaptic glutamate receptor fields were observed in control animals at a relatively low rate (5.47 ± 0.38 %, n=19) (Fig. 7A). In contrast, act^{E84K} mutants displayed frequent BRP puncta without a DGluRIII counterpart, or vice versa (Fig. 7B). Quantification of AZs and DGluRIII clusters from 3D-reconstructed synaptic boutons revealed a significant increase unapposed AZs in act^{E84K} mutants (control, 5.47 ± 0.38%, n=19; act^{E84K}, 8.98 ± 0.85 %, n=19; $p=0.0006$) (Fig. 7C). We also noted during our analysis that DGluRIII-labeled glutamate receptor fields in act^{E84K} mutants were often enlarged and less punctate compared to those found in control animals. As such, our data indicate the postsynaptic actin cytoskeleton plays a key regulatory role in synapse assembly, ensuring proper alignment of presynaptic release sites with postsynaptic receptor fields, in addition to its role in AZ spacing and density described above (Fig. 2).

AZ alignment to postsynaptic receptors at the *Drosophila* NMJ has previously been proposed to be regulated by cell adhesion molecules such as Neurexin-Neuroligin (Li et al., 2007; Banovic et al., 2010). We performed a genetic interaction analysis to determine

whether Actin 57B influences AZ assembly through a pathway dependent on the *Drosophila* neurexin homolog (DNrx). Quantification of AZ apposition in either heterozygote act^{E84K}/+ or nrx^{278}/+ alone revealed no significant increase in unapposed AZs compared to control (Fig. 7D). However, loss of one copy of *DNrx* in the act^{E84K}/+ background resulted in a significant increase in misaligned AZs to postsynaptic receptor fields (Fig. 7D; $p<0.05$). The genetic interaction between act^{E84K} and *DNrx* mutants suggest that the postsynaptic cytoskeleton may interface with transsynaptic signaling complexes to organize proper alignment of presynaptic release sites and postsynaptic receptor clusters.

Functional analysis of act^{E84K} mutants

Based on the defects in AZ alignment to postsynaptic receptors, we examined whether synaptic transmission was also disrupted in act^{E84K} and act^{E84K}/*Df(2R)Exel7166* mutants. Sharp electrode recordings were carried out in modified HL3 saline containing 1 mM Ca^{2+} at muscle fibers 6/7 of 3rd instar control and mutant larvae. Evoked neurotransmitter release was significantly decreased in the act^{E84K} mutant (Fig. 8A, B) (average excitatory junctional potential (EJP) amplitude in control: 33.5 ± 1.8 mV, n=6; act^{E84K}: 18.9 ± 1.7 mV, n=7; $p \leq 0.0001$). A reduction in evoked amplitude could be secondary to presynaptic defects such as reduced SV release or SV size, or postsynaptic defects such as reduced glutamate receptor density or sensitivity. Measurement of spontaneous miniature event amplitude revealed a reduction in the average size of the miniature excitatory junctional potential (mEJP or mini) compared to control (Fig. 8D, G, H) (control: 1.3 ± 0.1 mV, n=10; act^{E84K}: 0.8 ± 0.1 mV, n=11; p=0.001), indicating a postsynaptic defect. Consistent with the reduction in AZ number, mini frequency was also decreased in mutant animals (Fig. 8E, F) (control: 2.0 ± 0.1 Hz, n=10; act^{E84K}: 1.1 ± 0.2 Hz, n=11; p=0.001). In contrast, quantal content (the number of SVs released following an action potential) showed no significant difference (Fig. 8C) (control: 31.0 ± 2.2, n=6; act^{E84K}: 33.1 ± 1.8, n=7; p=0.4667), indicating a postsynaptic defect in act^{E84K} mutants. Consistently, ultrastructural analysis did not reveal any differences in SV size compared to control (Fig. 6F), arguing against a reduction in vesicular neurotransmitter content in act^{E84K} mutants. We next examined physiological defects in act^{E84K}/*Df(2R)Exel7166* transheterozygote larvae and compared them to *Df(2R)Exel7166*/+ controls. act^{E84K}/*Df(2R)Exel7166* mutants also displayed reduced evoked amplitude and spontaneous release frequency, with no change in quantal content (Fig. 8A-F). However, the *Df(2R)Exel7166*/+ heterozygote showed a dominant impairment in mini amplitude (Fig. 8G, H), making it difficult to compare to this phenotype to the act^{E84K} homozygous line. In summary, the impaired synaptic transmission in act^{E84K} mutants is consistent with the observed defects in glutamate receptor clustering, field size and apposition secondary to disruption of the postsynaptic cytoskeleton.

DISCUSSION

Using an unbiased genetic screen for regulators of synaptic growth and organization in *Drosophila*, we isolated a mutation in B that revealed a role for the postsynaptic cytoskeleton in regulating presynaptic AZ density and alignment with postsynaptic glutamate receptor fields. In act^{E84K} mutant animals, the organization of the postsynaptic compartment is severely disrupted, with prominent F-actin swirls and mislocalization of

spectrin, adducin and DLG. In addition to its critical role in postsynaptic cytoskeletal organization, Actin 57B is required for proper AZ spacing and alignment. These results indicate that the postsynaptic actin cytoskeleton is critical for establishing postsynaptic protein networks that control transsynaptic communication and coordinated synapse formation.

The *act*^{E84K} allele was isolated based on its striking presynaptic AZ organization defects. However, *Actin 57B* mRNA is expressed solely in muscle cells (Fyrberg et al., 1983; Tobin et al., 1990a), and its expression is regulated by MEF2, a muscle-specific transcription factor (Kelly et al., 2002; Elgar et al., 2008). Together with the defect in postsynaptic actin structure at the NMJ (Fig. 4), our data suggest that Actin 57B functions in the postsynaptic compartment to regulate presynaptic architecture. We were unable to perform rescue experiments using a wild-type Actin 57B construct expressed in the *act*^{E84K} background to unambiguously exclude a presynaptic contribution. We generated wild-type and E84K *Actin 57B* transgenes carrying either a N-terminal myc- or GFP-tag using phiC31 integrase-mediated targeted insertion (Groth et al., 2004). Although these tagged actin constructs were able to assemble normally into myofibril filaments, they did not properly integrate into the postsynaptic cytoskeleton, preventing a rescue-based analysis. Actin expression levels are tightly controlled, and transgenic expression may be insufficient to enrich the protein at NMJ. Alternatively, tagged actin constructs may disrupt normal incorporation of the protein into the postsynaptic cytoskeleton.

The location of the E84 residue in the actin crystal structure (Fig. 3) suggests that mutation of this site would impair binding to members of the CH domain superfamily. In agreement with this hypothesis, postsynaptic spectrin is severely mislocalized in *act*^{E84K} (Fig. 5). In addition, prior studies have revealed distinct phenotypes upon expression of α- and β-spectrin RNAi either presynaptically in the neuron or postsynaptically in the muscle. Phenotypes resulting from postsynaptic spectrin RNAi expression are similar to what we have observed in *act*^{E84K} mutant animals (Pielage et al., 2006). Postsynaptic knockdown leads to mislocalization of DLG, impaired SSR formation, and aberrant AZ spacing. In contrast, neuronal-specific knockdown of presynaptic spectrin results in a very different synaptic retraction phenotype, as it is essential for synapse stabilization (Pielage et al., 2005). Synaptic retraction was not observed in *act*^{E84K} mutants (data not shown), suggesting the presynaptic actin-spectrin network is intact in this mutant. These results are consistent with *Actin 5C* and *Actin 42A* contributing to the presynaptic actin cytoskeleton, which are unaffected by a mutation in the *Actin 57B* isoform. In addition, electrophysiological characterization demonstrated a postsynaptic defect in *act*^{E84K} mutants, in contrast to clear phenotypes induced by presynaptic spectrin RNAi expression or pharmacological disruption of presynaptic actin in cultured hippocampal neurons. Presynaptic spectrin RNAi expression leads to impaired presynaptic release with a reduction in mini frequency and quantal content. These functional defects are correlated with the severity of synapse disassembly (Pielage et al., 2005). On the other hand, pharmacological disruption of presynaptic actin allows for functional analysis in the absence of the added factor of synapse retraction (Morales et al., 2000). Using this approach, disruption of presynaptic actin has been shown to increase neurotransmitter release probability as manifested in a decreased paired pulse

ratio. These studies collectively indicate a role for the presynaptic actin-spectrin network in regulating neurotransmitter release, in contrast to what we observe in act^{E84K} mutants. The amplitude of evoked release events in act^{E84K} mutants is reduced due to a decrease in the size of individual minis in act^{E84K}, with no changes in quantal content (Fig. 8). These results indicate a postsynaptic functional defect in act^{E84K} mutants, likely due to impaired pre- and post-synaptic alignment and clustering of glutamate receptors. We also found that postsynaptic glutamate receptor fields in act^{E84K} mutants lacked their normal punctate staining pattern, often with abnormal elongation. Interestingly, both the actin-spectrin network and DLG have been shown to regulate glutamate receptor cluster size. Reduction of the postsynaptic actin-spectrin rich domain and disruption of its organization result in an increase in glutamate receptor cluster size (Pielage et al., 2006; Ramachandran et al., 2009). In addition, DLG has been shown to control glutamate receptor cluster size in a complex with the proteins Metro and DLin-7 (Karunanithi et al., 2002; Bachmann et al., 2010). Taken together, the severe disruption of the postsynaptic actin cytoskeleton seen in act^{E84K} mutants may disrupt multiple pathways required to organize the PSD and regulate glutamate receptor cluster size.

Mapping of the isolated Actin 57B allele revealed a point mutation in a highly conserved amino acid within the actin superfamily (Fig. 3). Glutamate E84 has previously been shown to participate in binding to the CH domain protein superfamily (Honts et al., 1994; McGough et al., 1994; Hanein et al., 1997; Hodgkinson et al., 1997; Moores et al., 2000; Galkin, 2002; Sutherland-Smith et al., 2003). Disruption of the CH domain-binding site in Actin 57B could disrupt multiple protein networks. Based on the findings reported here, the interaction with postsynaptic spectrin is likely to be impaired in act^{E84K} mutants. The assembly of prominent F-actin swirls concentrating around the NMJ (Fig. 4) provided the first indication, as β-$spec^{em6}$ mutants display a similar phenotype (Ramachandran et al., 2009). Loss of α-spectrin localization to the postsynaptic SSR region (Fig. 5), as well as similarities with postsynaptic spectrin RNAi, supports this model. In addition to spectrin, Adducin (*Hts*) is a member of the spectrin cytoskeleton, facilitating actin-spectrin binding (Gardner and Bennett, 1987; Matsuoka et al., 2000). We found that *hts* mutants displayed a rearrangement of the postsynaptic actin cytoskeleton different from act^{E84K} or β-$spec^{em6}$, exhibiting reduced actin NMJ localization and aberrant F-actin rings throughout the muscle (Fig. 5).

In addition to disruptions of the postsynaptic cytoskeleton, a number of defects in synaptic architecture were found in act^{E84K} mutants, including aberrant glutamate receptor clustering and AZ spacing and density. As discussed above, postsynaptic but not presynaptic spectrin has been shown to regulate AZ size and spacing (Pielage et al., 2006). Postsynaptic expression of β-spectrin RNAi disrupts glutamate receptor clustering and AZ spacing in a similar fashion to that observed in act^{E84K} mutants. Pielage et al. (2006) proposed that the postsynaptic actin-spectrin skeleton forms a grid-like network, providing regular spacing for cell adhesion molecules to organize pre- and post-synaptic densities. Interestingly, apposition defects have also been described after loss of the cell adhesion proteins Neurexin-Neuroligin and Teneurins (Li et al., 2007; Banovic et al., 2010; Mosca et al., 2012). The *Drosophila* genome encodes one DNrx and four DNlgs (of which only two have been

analyzed) (Li et al., 2007; Banovic et al., 2010; Chen et al., 2010; Sun et al., 2011). DNrx and DNlg2 localize primarily presynaptic, while DNlg1 expression is muscle-specific. Similarly, Teneurins (Ten) are transmembrane proteins required for synapse organization (Mosca et al., 2012). Ten-a localizes to the presynaptic membrane, whereas Ten-m is predominantly concentrated at the SSR. Upon loss of either the Neurexin-Neuroligin complex or Teneurins, alignment of BRP and DGluRIII is perturbed, and ultrastructural analysis reveals aberrant AZ structure. Although both cell adhesion complexes function at the NMJ, AZ apposition has been proposed to be mainly regulated by the Neurexin-Neuroligin complex, while Teneurins primarily organize the cytoskeleton (Mosca et al., 2012). Neuroligin binds PSD-95 in mammals and recruits DLG in *Drosophila* (Irie, 1997; Banovic et al., 2010; Mosca et al., 2012), suggesting that the Neurexin-Neroligin complex is a strong candidate to couple the postsynaptic cytoskeleton with presynaptic AZ organization. Indeed, we found that act^{E84K} and *neurexin* mutants displayed genetic interactions for AZ-postsynaptic receptor alignment phenotypes. Future studies will examine if Teneurins also interface with the actin cytoskeleton to regulate synapse assembly. In summary, the analysis of act^{E84K} mutants reveals a key role for the postsynaptic actin-spectrin cytoskeleton in organizing transsynaptic signaling to regulate presynaptic AZ spacing, density and alignment.

EXPERIMENTAL METHODS

Genetic screen and *Drosophila* stocks

Five rounds of ethyl methanesulfonate (EMS) mutagenesis was performed, with 500 isogenized control CS males fed 25 mM EMS for each round. Mutagenized males were crossed to virgins of the second chromosome balancer ln(2LR)Gla, wg^{Gla-1}/CyO,GFP. Single male progeny were crossed to ln(2LR)Gla, wg^{Gla-1}/CyO,GFP, and stocks of the mutagenized chromosome balanced with CyO,GFP were established. Homozygous mutant non-GFP 3rd instar larvae from each stock were dissected and stained using anti-Bruchpilot and anti-GluRIII antibodies directly labeled with Alexa Fluors 555 and 488, respectively (Life Technologies, Grand Island, NY, USA). Bloomington stock BL1401 wg^{Sp-1} Bl^1 L^{rm} Bc^1 Pu^2 Pin^B/SM5 was used for recombination mapping, followed by deficiency mapping and PCR screening. For further analysis of act^{E84K} mutants, homozygous act^{E84K}, act^{E84K}/*Df(2R)Exel7166* and age-matched isogenized Canton-S or *Df(2R)Exel7166*/+ control larvae were reared on molasses plates with yeast paste. Adult flies were allowed to lay eggs for 16 hr and GFP-negative 1st instar larvae were transferred onto fresh plates after 24 hr. 3rd instar larvae were dissected 5 days after the first transfer.

Immunohistochemistry

Age-matched control and mutant 3rd instar larvae were dissected in ice-cold Ca^{2+}-free HL3.1 saline (Feng et al., 2004) and fixed for 30 min in HL3.1 containing 4% formaldehyde. Samples were washed in PBS followed by PBX (0.3% Triton X-100 in PBS) before antibody staining. Samples were mounted in either Vectashield mounting medium (Vector Laboratories, Burlingame, CA, USA) or Prolong Gold antifade reagent (Life Technologies, Grand Island, NY, USA). The primary antibodies used include: mouse anti-Bruchpilot, 1:250 (Wagh et al., 2006, obtained from Developmental Studies Hybridoma

Bank (DSHB), The Univ. of Iowa, Iowa, USA); rabbit anti-GluRIII, 1:1000 (Marrus, 2004); mouse anti-α-spectrin, 1:50 (DSHB); rabbit anti-β-spectrin, 1:500 (gift from R. Dubreuil); mouse anti-DLG, 1:1000 (DSHB); mouse anti-adducin, 1:50 (DSHB); DyLight 649 conjugated anti-horseradish peroxidase, 1:4000 (Jackson Immunoresearch, West Grove, PA, USA). Secondary antibodies were conjugated to Alexa-488 or Rhodamine Red-X (Jackson Immunoresearch). Alexa 488 or Rhodamine conjugated phalloidin was used to stain F-actin (Life Technologies).

Confocal imaging and quantification

Larvae were imaged on a Zeiss Axioplan microscope equipped with a LSM510 laser scanning head (Carl Zeiss, Thornwood, NY, USA) or a PerkinElmer Ultraview Vox spinning disk confocal microscope (PerkinElmer, Waltham, MA, USA) using the following Zeiss objectives: Plan-Neofluar 40x/1.30 Oil DIC, Plan-Apochromat 40x/1.30 Oil DIC (UV) VIS-IR, Plan-Apochromat 63x/1.40 Oil DIC, Plan-Neofluar 100x/1.30 Oil. Images were acquired with either Pascal (Carl Zeiss) or Volocity software (PerkinElmer). The postsynaptic actin cytoskeleton was imaged at muscle 12/13 of segments A2-A4. Quantification of AZ phenotypes was performed on NMJs of muscle 4 of segments A3-A4. For quantification of AZ number and alignment, images were deconvoluted prior to quantification using Volocity analysis software. AZ number per bouton, bouton volume and number of boutons were quantified. For alignment, the number of unapposed BRP and/or GluRIII puncta was counted manually using the 3D image function of Volocity software. Statistical significance between two samples was calculated using an unpaired Student's *t*-test. For analysis of more than two samples, ANOVA was used with a Dunnett's post-hoc test to compare to control and a Bonferroni post-hoc test to compare genotypes. Cumulative probability distributions were compared with the Kolmogorov-Smirnov test (Prism software, GraphPad, La Jolla, CA, USA). For the figures and text, ****< 0.0001, *** < 0.001, ** 0.001 to 0.01, * 0.01 to 0.05, ns > 0.05.

STORM imaging

Age-matched larvae were dissected as described above, fixed in 4% paraformaldehyde in PBS and permeabilized in 0.2% PBX. Staining and imaging was done as described previously (Xu et al., 2013). Briefly, primary antibodies were added to blocking buffer (3% bovine serum albumin in 0.2% PBX) overnight at 4°C, followed by 1 hr incubation with custom labeled secondary antibodies in blocking buffer. The secondary antibodies were labeled with photoswitchable Alexa 647 dye for STORM imaging. STORM imaging was performed on a Nikon Eclipse Ti-U inverted optical microscope. The dyes were activated by 405-nm laser (CUBE 405-50C; Coherent) and imaged with 656-nm laser (CL656-300; CrystaLaser). A 660dcxr (extended reflectivity dichroic, Chroma) was used as the dichroic mirror and an ET705/72M band-pass filter (Chroma) was used as the emission filter. For 3D STORM imaging, a cylindrical lens was inserted into the imaging path (Huang et al, 2008). Continuous illumination of 656-nm laser (~2 kW/cm^2) was used to excite fluorescence from Alexa647 molecules and switch them into the dark state for STORM imaging. Continuous illumination of the 405-nm laser was used to reactivate the fluorophores to the emitting state. The power of the activation lasers (typical range 0-1 W/cm^2) was adjusted during image acquisition so that at any given instant, only a small optically resolvable fraction of

the fluorophores in the sample were in the emitting state. A typical STORM image was generated from a sequence of about 60,000 image frames at a frame rate of 60 Hz. The recorded STORM movie was analyzed according to previously described methods (Huang et al, 2008; Xu et al., 2013).

Electron Microscopy

Age-matched control and mutant 3rd instar larvae were processed as previously described (Akbergenova and Bykhovskaia, 2009). Dissected larvae were fixed in 1% glutaraldehyde, 4% formaldehyde, 0.1 M sodium cacodylate for 3 hr at 4°C. Samples were washed in HL3.1 for 1 hr, post-fixed for 30 min in 1% osmium tetroxide, followed by a 20 min wash in distilled water. After dehydration through a graded series of ethanol and acetone, samples were embedded in Embed 812 epoxy resin (Electron Microscopy Sciences). Thin sections (50–60 nm) were collected on Formvar/carbon coated copper slot grids, and contrasted with 2% uranyl acetate and lead citrate.

Electrophysiology

Analysis of age-matched 3rd instar larvae was performed in modified HL3 saline (70 mM NaCl, 5mM KCl, 4 mM $MgCl_2$, 1 mM $CaCl_2$, 10 mM $NaHCO_3$, 115 mM sucrose, 5 mM HEPES, pH 7.2) at muscle fiber 6 of abdominal segment A3. To record evoked EJPs, segmental nerves were severed from the ventral nerve cord and stimulated using a programmable pulse generator (Master-8; AMPI, Jerusalem, Israel). Recordings from muscles that exhibited input resistance <5 MΩ were excluded from the analysis. pCLAMP software (Axon Instruments, Foster City, CA, USA) was used for data acquisition and analysis. Statistical analysis was performed using Prism software (GraphPad, La Jolla, CA, USA), and error bars represent SEM. An unpaired Student's *t*-test was used to calculate significance between two samples.

Acknowledgments

This work was supported by NIH grant NS40296 to J.T.L.

Abbreviations

NMJ	neuromuscular junction
EJP	excitatory junctional potential
Dm	Drosophila melanogaster
SEM	standard error of the mean
HRP	horse radish peroxidase
AZ	active zone
SSR	subsynaptic reticulum
SV	synaptic vesicle
EM	electron microscopy

REFERENCES

Akbergenova Y, Bykhovskaia M. Molecular and Cellular Neuroscience. Molecular and Cellular Neuroscience. 2009; 40:199–206. [PubMed: 19026748]

Atwood HL, Govind CK, Wu CF. Differential ultrastructure of synaptic terminals on ventral longitudinal abdominal muscles in Drosophila larvae. J Neurobiol. 1993; 24:1008–1024. [PubMed: 8409966]

Bachmann A, Kobler O, Kittel RJ, Wichmann C, Sierralta J, Sigrist SJ, Gundelfinger ED, Knust E, Thomas U. A Perisynaptic Menage a Trois between Dlg, DLin-7, and Metro Controls Proper Organization of Drosophila Synaptic Junctions. J Neurosci. 2010; 30:5811–5824. [PubMed: 20427642]

Baines AJ. The spectrin–ankyrin–4.1–adducin membrane skeleton: adapting eukaryotic cells to the demands of animal life. Protoplasma. 2010; 244:99–131. [PubMed: 20668894]

Banovic D, Khorramshahi O, Owald D, Wichmann C, Riedt T, Fouquet W, Tian R, Sigrist SJ, Aberle H. Drosophila neuroligin 1 promotes growth and postsynaptic differentiation at glutamatergic neuromuscular junctions. Neuron. 2010; 66:724–738. [PubMed: 20547130]

Bennett V, Baines AJ. Spectrin and ankyrin-based pathways: metazoan inventions for integrating cells into tissues. Physiol Rev. 2001; 81:1353–1392. [PubMed: 11427698]

Bennett V, Davis J. Spectrin and ankyrin in brain. Cell Motil. 1983; 3:623–633. [PubMed: 6229335]

Bennett V, Davis J, Fowler WE. Brain spectrin, a membrane-associated protein related in structure and function to erythrocyte spectrin. Nature. 1982; 299:126. [PubMed: 7110333]

Bennett V, Gardner K, Steiner JP. Brain adducin: a protein kinase C substrate that may mediate site-directed assembly at the spectrin-actin junction. J Biol Chem. 1988; 263:5860–5869. [PubMed: 2451672]

Bennett V, Gilligan DM. The spectrin-based membrane skeleton and micron-scale organization of the plasma membrane. Annu Rev Cell Biol. 1993; 9:27–66. [PubMed: 8280463]

Bennett V, Lambert S. The spectrin skeleton: from red cells to brain. J Clin Invest. 1991; 87:1483–1489. [PubMed: 1850755]

Budnik V, Koh Y, Guan B, Hartmann B, Hough C. Regulation of synapse structure and function by the Drosophila tumor suppressor gene dlg. Neuron. 1996

Burn TC, Vigoreaux JO, Tobin SL. Alternative 5C actin transcripts are localized in different patterns during Drosophila embryogenesis. Dev Biol. 1989; 131:345–355. [PubMed: 2492241]

Chen J, Mizushige T, Nishimune H. Active zone density is conserved during synaptic growth but impaired in aged mice. J Comp Neurol. 2011; 520:434–452. [PubMed: 21935939]

Chen K, Gracheva EO, Yu S-C, Sheng Q, Richmond J, Featherstone DE. Neurexin in Embryonic Drosophila Neuromuscular Junctions Mei L, ed. PLoS ONE. 2010; 5:e11115. [PubMed: 20559439]

Chen K, Merino C, Sigrist SJ, Featherstone DE. The 4.1 protein coracle mediates subunit- selective anchoring of Drosophila glutamate receptors to the postsynaptic actin cytoskeleton. J Neurosci. 2005; 25:6667–6675. [PubMed: 16014728]

Cingolani LA, Goda Y. Actin in action: the interplay between the actin cytoskeleton and synaptic efficacy. Nat Rev Neurosci. 2008; 9:344–356. [PubMed: 18425089]

Clarke GL, Chen J, Nishimune H. Presynaptic Active Zone Density during Development and Synaptic Plasticity. Front Mol Neurosci. 2012; 5:12. [PubMed: 22438837]

Coyle IP, Koh Y-H, Lee W-CM, Slind J, Fergestad T, Littleton JT, Ganetzky B. Nervous wreck, an SH3 adaptor protein that interacts with Wsp, regulates synaptic growth in Drosophila. Neuron. 2004; 41:521–534. [PubMed: 14980202]

Dalva MB, McClelland AC, Kayser MS. Cell adhesion molecules: signalling functions at the synapse. Nat Rev Neurosci. 2007; 8:206–220. [PubMed: 17299456]

Dickman DK, Lu Z, Meinertzhagen IA, Schwarz TL. Altered Synaptic Development and Active Zone Spacing in Endocytosis Mutants. Current Biology. 2006; 16:591–598. [PubMed: 16546084]

Dillon C, Goda Y. The actin cytoskeleton: integrating form and function at the synapse. Annu Rev Neurosci. 2005; 28:25–55. [PubMed: 16029114]

Doussau F, Augustine GJ. The actin cytoskeleton and neurotransmitter release: an overview. Biochimie. 2000; 82:353–363. [PubMed: 10865123]

Dubreuil RR, Das A. Squire LR. Spectrin: Organization and Function in Neurons. Encyclopedia of Neuroscience. 2009:213–218.

Academic Press, Oxford; Elgar, SJ.; Han, J.; Taylor, MV. mef2 activity levels differentially affect gene expression during Drosophila muscle development. Proc Natl Acad Sci USA. 2008; 105:918–923. [PubMed: 18198273]

Enneking E-M, Kudumala SR, Moreno E, Stephan R, Boerner J, Godenschwege TA, Pielage J. Bellen HJ. Transsynaptic Coordination of Synaptic Growth, Function, and Stability by the L1-Type CAM Neuroglian. PLoS Biol. 2013; 11:e1001537. [PubMed: 23610557]

Featherstone DE, Davis WS, Dubreuil RR, Broadie K. Drosophila alpha- and beta-spectrin mutations disrupt presynaptic neurotransmitter release. J Neurosci. 2001; 21:4215–4224. [PubMed: 11404407]

Feng Y, Ueda A, Wu C-F. A modified minimal hemolymph-like solution, HL3. 1, for physiological recordings at the neuromuscular junctions of normal and mutant Drosophila larvae. J Neurogenet. 2004; 18:377–402. [PubMed: 15763995]

Fyrberg EA, Fyrberg CC, Biggs JR, Saville D, Beall CJ, Ketchum A. Functional nonequivalence of Drosophila actin isoforms. Biochem Genet. 1998; 36:271–287. [PubMed: 9791722]

Fyrberg EA, Kindle KL, Davidson N, Kindle KL. The actin genes of Drosophila: a dispersed multigene family. Cell. 1980; 19:365–378. [PubMed: 6244106]

Fyrberg EA, Mahaffey JW, Bond BJ, Davidson N. Transcripts of the six Drosophila actin genes accumulate in a stage- and tissue-specific manner. Cell. 1983; 33:115–123. [PubMed: 6432334]

Galkin VE. The utrophin actin-binding domain binds F-actin in two different modes: implications for the spectrin superfamily of proteins. J Cell Biol. 2002; 157:243–251. [PubMed: 11956227]

Gardner K, Bennett V. Modulation of spectrin-actin assembly by erythrocyte adducin. Nature. 1987; 328:359–362. [PubMed: 3600811]

Giagtzoglou N, Ly C, Bellen H. Cell adhesion, the backbone of the synapse:“vertebrate” and ‘invertebrate’ perspectives. Cold Spring Harbor Perspectives in Biology. 2009; 1

Graf ER, Daniels RW, Burgess RW, Schwarz TL, DiAntonio A. Rab3 Dynamically Controls Protein Composition at Active Zones. Neuron. 2009; 64:663–677. [PubMed: 20005823]

Groth AC, Fish M, Nusse R, Calos MP. Construction of transgenic Drosophila by using the site-specific integrase from phage phiC31. Genetics. 2004; 166:1775–1782. [PubMed: 15126397]

Hanein D, Matsudaira P, DeRosier DJ. Evidence for a conformational change in actin induced by fimbrin (N375) binding. J Cell Biol. 1997; 139:387–396. [PubMed: 9334343]

Hodgkinson JL, EL-Mezgueldi M, Craig R, Vibert P, Marston SB, Lehman W. 3-D image reconstruction of reconstituted smooth muscle thin filaments containing calponin: visualization of interactions between F-actin and calponin. J Mol Biol. 1997; 273:150–159. [PubMed: 9367753]

Honts JE, Sandrock TS, Brower SM, O'Dell JL, Adams AE. Actin mutations that show suppression with fimbrin mutations identify a likely fimbrin-binding site on actin. J Cell Biol. 1994; 126:413–422. [PubMed: 8034742]

Huang B, Wang W, Bates M, Zhuang X. Three-dimensional super-resolution imaging by stochastic optical reconstruction microscopy. Science. 2008; 319:810–813. [PubMed: 18174397]

Irie M. Binding of Neuroligins to PSD-95. Science. 1997; 277:1511–1515. [PubMed: 9278515]

Karunanithi S, Marin L, Wong K, Atwood HL. Quantal size and variation determined by vesicle size in normal and mutant Drosophila glutamatergic synapses. J Neurosci. 2002; 22:10267–10276. [PubMed: 12451127]

Kelly KK, Meadows SM, Cripps RM. Drosophila MEF2 is a direct regulator of Actin57B transcription in cardiac, skeletal, and visceral muscle lineages. Mech Dev. 2002; 110:39–50. [PubMed: 11744367]

Kuhlman PA, Hughes CA, Bennett V, Fowler VM. A new function for adducin. Calcium/calmodulin-regulated capping of the barbed ends of actin filaments. J Biol Chem. 1996; 271:7986–7991. [PubMed: 8626479]

Lahey T, Gorczyca M, Jia XX, Budnik V. The Drosophila tumor suppressor gene dlg is required for normal synaptic bouton structure. Neuron. 1994; 13:823–835. [PubMed: 7946331]

Li J, Ashley J, Budnik V, Bhat MA. Crucial Role of Drosophila Neurexin in Proper Active Zone Apposition to Postsynaptic Densities, Synaptic Growth, and Synaptic Transmission. Neuron. 2007; 55:741–755. [PubMed: 17785181]

Li X, Matsuoka Y, Bennett V. Adducin preferentially recruits spectrin to the fast growing ends of actin filaments in a complex requiring the MARCKS-related domain and a newly defined oligomerization domain. J Biol Chem. 1998; 273:19329–19338. [PubMed: 9668123]

Marchesi VT, Steers E. Selective solubilization of a protein component of the red cell membrane. Science. 1968; 159:203–204. [PubMed: 5634911]

Marrus SB. Differential Localization of Glutamate Receptor Subunits at the Drosophila Neuromuscular Junction. Journal of Neuroscience. 2004; 24:1406–1415. [PubMed: 14960613]

Matsuoka Y, Li X, Bennett V. Adducin: structure, function and regulation. Cell Mol Life Sci. 2000; 57:884–895. [PubMed: 10950304]

McGough A, Way M, DeRosier D. Determination of the alpha-actinin-binding site on actin filaments by cryoelectron microscopy and image analysis. J Cell Biol. 1994; 126:433–443. Available at: http://jcb.rupress.org/content/126/2/433.full.pdf#page=1&view=FitH. [PubMed: 8034744]

Meinertzhagen IA, Govind CK, Stewart BA, Carter JM, Atwood HL. Regulated spacing of synapses and presynaptic active zones at larval neuromuscular junctions in different genotypes of the flies Drosophila and Sarcophaga. J Comp Neurol. 1998; 393:482–492. [PubMed: 9550153]

Moores CA, Keep NH, Kendrick-Jones J. Structure of the utrophin actin-binding domain bound to F-actin reveals binding by an induced fit mechanism. J Mol Biol. 2000; 297:465–480. [PubMed: 10715214]

Morales M, Colicos MA, Goda Y. Actin-dependent regulation of neurotransmitter release at central synapses. Neuron. 2000; 27:539–550. [PubMed: 11055436]

Mosca TJ, Hong W, Dani VS, Favaloro V, Luo L. Trans-synaptic Teneurin signalling in neuromuscular synapse organization and target choice. Nature. 2012:1–7.

Nelson JC, Stavoe AKH, Colón-Ramos DA. The actin cytoskeleton in presynaptic assembly. celladhesion. 2013; 7

Nishimune H. Active zones of mammalian neuromuscular junctions: formation, density, and aging. Annals of the New York Academy of Sciences. 2012; 1274:24–32. [PubMed: 23252894]

Nunes P, Haines N, Kuppuswamy V, Fleet DJ, Stewart BA. Synaptic vesicle mobility and presynaptic F-actin are disrupted in a N-ethylmaleimide-sensitive factor allele of Drosophila. Mol Biol Cell. 2006; 17:4709–4719. [PubMed: 16914524]

Petersen SA, Fetter RD, Noordermeer JN, Goodman CS, DiAntonio A. Genetic analysis of glutamate receptors in Drosophila reveals a retrograde signal regulating presynaptic transmitter release. Neuron. 1997; 19:1237–1248. [PubMed: 9427247]

Pielage J, Bulat V, Zuchero JB, Fetter RD, Davis GW. Hts/Adducin Controls Synaptic Elaboration and Elimination. Neuron. 2011; 69:1114–1131. [PubMed: 21435557]

Pielage J, Fetter RD, Davis GW. Presynaptic spectrin is essential for synapse stabilization. Curr Biol. 2005; 15:918–928. [PubMed: 15916948]

Pielage J, Fetter RD, Davis GW. A postsynaptic spectrin scaffold defines active zone size, spacing, and efficacy at the Drosophila neuromuscular junction. J Cell Biol. 2006; 175:491–503. [PubMed: 17088429]

Ramachandran P, Barria R, Ashley J, Budnik V. A critical step for postsynaptic F-actin organization: Regulation of Baz/Par-3 localization by aPKC and PTEN. Devel Neurobio. 2009; 69:583–602.

Reiff DF, Thiel PR, Schuster CM. Differential regulation of active zone density during long-term strengthening of Drosophila neuromuscular junctions. Journal of Neuroscience. 2002; 22:9399–9409. [PubMed: 12417665]

Ruiz-Canada C, Ashely J, Moeckel-Cole S, Drier E, Yin J, Budnik V. New synaptic bouton formation is disrupted by misregulation of microtubule stability in aPKC mutants. Neuron. 2004; 42:567–580. [PubMed: 15157419]

Sigrist SJ, Schmitz D. Structural and functional plasticity of the cytoplasmic active zone. Current Opinion in Neurobiology. 2011; 21:144–150. [PubMed: 20832284]

Sigrist SJ, Thiel PR, Reiff DF, Schuster CM. The postsynaptic glutamate receptor subunit DGluR-IIA mediates long-term plasticity in Drosophila. Journal of Neuroscience. 2002; 22:7362–7372. [PubMed: 12196557]

Stewart BA, Schuster CM, Goodman CS, Atwood HL. Homeostasis of synaptic transmission in Drosophila with genetically altered nerve terminal morphology. J Neurosci. 1996; 16:3877–3886. [PubMed: 8656281]

Südhof TC. Neurotransmitter release: the last millisecond in the life of a synaptic vesicle. Neuron. 2013; 80:675–690. [PubMed: 24183019]

Sun M, Xie W. Cell adhesion molecules in Drosophila synapse development and function. Sci China Life Sci. 2012; 55:20–26. [PubMed: 22314487]

Sun M, Xing G, Yuan L, Gan G, Knight D, With SI, He C, Han J, Zeng X, Fang M, Boulianne GL, Xie W. Neuroligin 2 Is Required for Synapse Development and Function at the Drosophila Neuromuscular Junction. J Neurosci. 2011; 31:687–699. [PubMed: 21228178]

Sutherland-Smith AJ, Moores CA, Norwood FLM, Hatch V, Craig R, Kendrick-Jones J, Lehman W. An Atomic Model for Actin Binding by the CH Domains and Spectrin-repeat Modules of Utrophin and Dystrophin. J Mol Biol. 2003; 329:15–33. [PubMed: 12742015]

Tillack TW, Marchesi SL, Marchesi VT, Steers E. A comparative study of spectrin: a protein isolated from red blood cell membranes. Biochim Biophys Acta. 1970; 200:125–131. [PubMed: 4983327]

Tobin S, Zulauf E, Sanchez F, Craig E. Multiple actin-related sequences in the Drosophila melanogaster genome. Cell. 1980

Tobin SL, Cook PJ, Burn TC. Transcripts of individual Drosophila actin genes are differentially distributed during embryogenesis. Dev Genet. 1990a; 11:15–26. [PubMed: 1694472]

Tobin SL, Cook PJ, Burn TC. Transcripts of individual Drosophila actin genes are differentially distributed during embryogenesis. Dev Genet. 1990b; 11:15–26. [PubMed: 1694472]

Valakh V, Naylor SA, Berns DS, DiAntonio A. A large-scale RNAi screen identifies functional classes of genes shaping synaptic development and maintenance. Dev Biol. 2012:1–9.

Viquez NM, Fuger P, Valakh V, Daniels RW, Rasse TM, Diantonio A. PP2A and GSK-3 Act Antagonistically to Regulate Active Zone Development. Journal of Neuroscience. 2009; 29:11484–11494. [PubMed: 19759297]

Wagh D, Rasse T, Asan E, Hofbauer A, Schwenkert I, Durrbeck H, Buchner S, Dabauvalle M, Schmidt M, Qin G. Bruchpilot, a Protein with Homology to ELKS/CAST, Is Required for Structural Integrity and Function of Synaptic Active Zones in Drosophila. Neuron. 2006; 49:833–844. [PubMed: 16543132]

Wairkar YP, Toda H, Mochizuki H, Furukubo-Tokunaga K, Tomoda T, Diantonio A. Unc-51 Controls Active Zone Density and Protein Composition by Downregulating ERK Signaling. J Neurosci. 2009; 29:517–528. [PubMed: 19144852]

Wang S, Yang J, Tsai A, Kuca T, Sanny J, Lee J, Dong K, Harden N, Krieger C. Drosophila adducin regulates Dlg phosphorylation and targeting of Dlg to the synapse and epithelial membrane. Dev Biol. 2011:1–12.

Xu K, Zhong G, Zhuang X. Actin, Spectrin, and Associated Proteins Form a Periodic Cytoskeletal Structure in Axons. Science. 2013; 339:452–456. [PubMed: 23239625]

Yue L, Spradling AC. hu-li tai shao, a gene required for ring canal formation during Drosophila oogenesis, encodes a homolog of adducin. Genes & Development. 1992; 6:2443–2454. [PubMed: 1340461]

Zito K, Parnas D, Fetter RD, Isacoff EY, Goodman CS. Watching a synapse grow: noninvasive confocal imaging of synaptic growth in Drosophila. Neuron. 1999; 22:719–729. [PubMed: 10230792]

Highlights

- An E84K mutation was identified in the spectrin binding domain of Actin 57B.
- Disruption of the postsynaptic cytoskeleton alters active zone organization.
- Loss of the actin-spectrin network disrupts active zone-receptor alignment.
- *act*^{E84K} genetically interacts with the neurexin transsynaptic signaling complex.

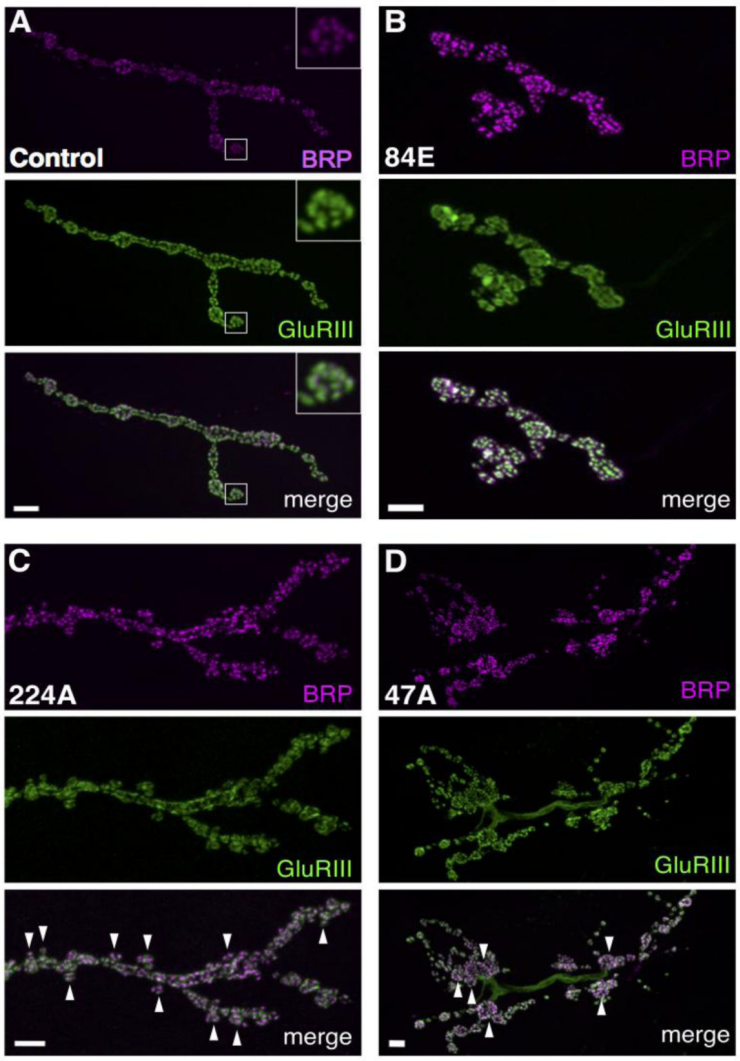

Fig. 1.

Representative muscle 4 NMJ morphology for mutant alleles isolated in an EMS screen for synaptic development defects. (A) Example of a control muscle 4 NMJ stained with BRP and GluRIII. The normal alignment of AZ to postsynaptic glutamate receptors is exemplified in the high magnification inset of the boxed region. In a forward genetic EMS screen for synaptic mutants, we identified 5 strains with defects in AZ number or spacing, 10 synaptic overgrowth mutants, 3 synaptic undergrowth mutants, 6 lines displaying excessive satellite bouton formation and 5 lines showing more complex morphological defects. (B) Homozygous 84E mutant larvae display enlarged glutamate receptor fields and satellite bouton overgrowth. Note the diffuse staining (green) for GluRIII compared to the discrete puncta found apposed to wild-type active zones. (C) Homozygous 224A mutant larvae display abnormal synaptic growth with small boutons (arrowheads) sprouting abnormally off the main axonal branch. (D) Homozygous 47A mutant larvae display synaptic overgrowth with numerous abnormally enlarged boutons (arrowheads). Scale bar, 5 μM.

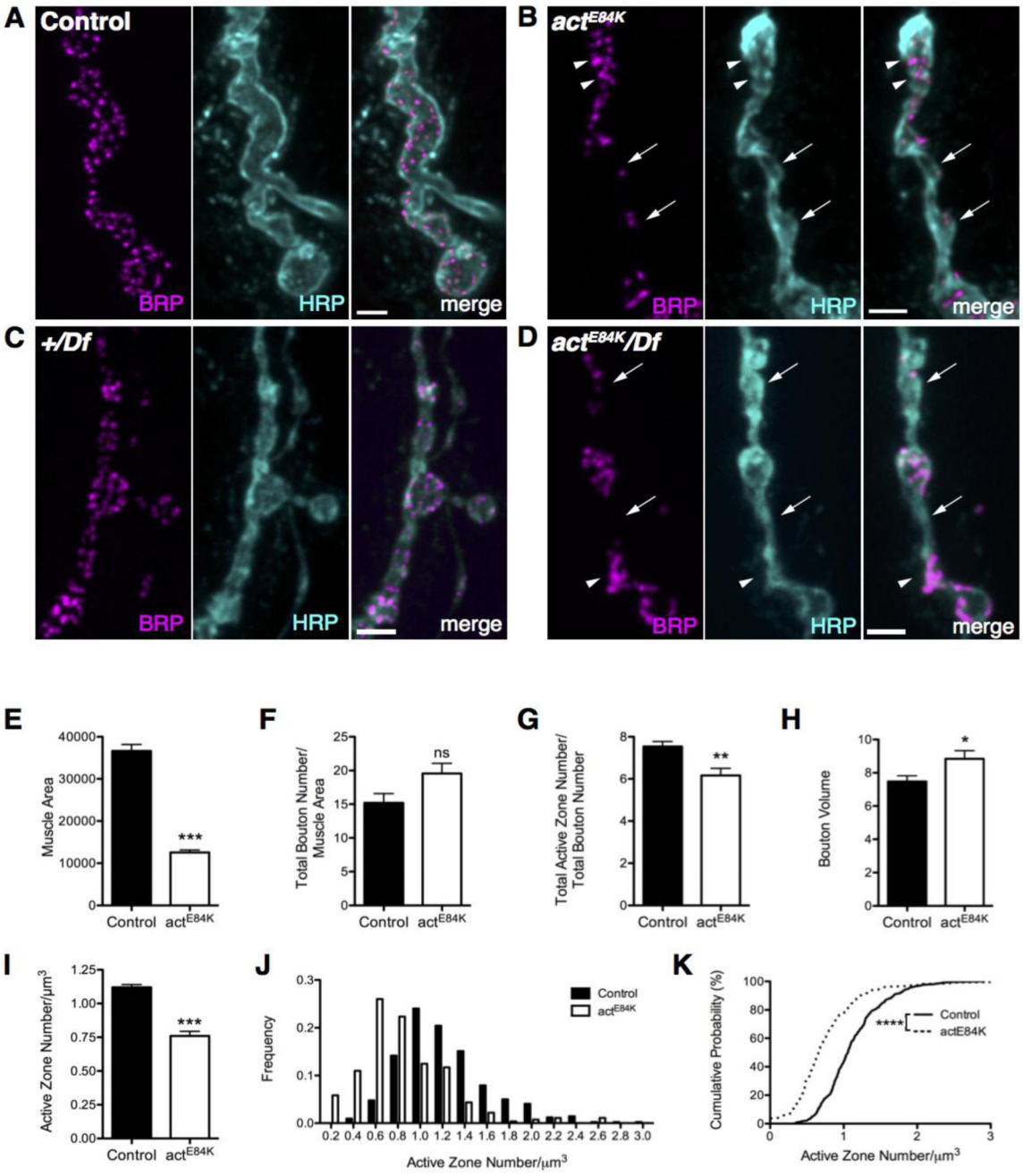

Fig 2.

Actin 57B regulates AZ spacing and alignment. (A) BRP puncta are regularly distributed in control boutons. (B) AZ spacing is disrupted in *act*^{E84K}, with some boutons nearly devoid of AZs (arrows) and others with clumping of AZs (arrowheads). (C) BRP puncta maintain their normal spacing in boutons of *Df(2R)Exel7166*/+ heterozygous animals. (D) AZ distribution is disrupted in *act*^{E84K}/*Df(2R)Exel7166* transheterozygous mutants, with some boutons lacking AZs (arrows) and others displaying AZ clumping (arrowheads). (E) Muscle surface area is reduced in *act*^{E84K} larvae compared to age-matched control. (F) Total bouton number per muscle surface area is not significantly different in *act*^{E84K} compared to control. (G) AZ

density per total bouton number is decreased in act^{E84K}. (H) Bouton volume (in μm^3) is increased in act^{E84K} mutants compared to control. (I) The number of AZs per bouton volume (in μm^3) is significantly decreased in act^{E84K}. (J, K) Frequency distributions of AZ number per bouton volume reveal a significant shift towards fewer AZs per volume in act^{E84K}. Mean and SEM are indicated. Scale bar, 2 μm.

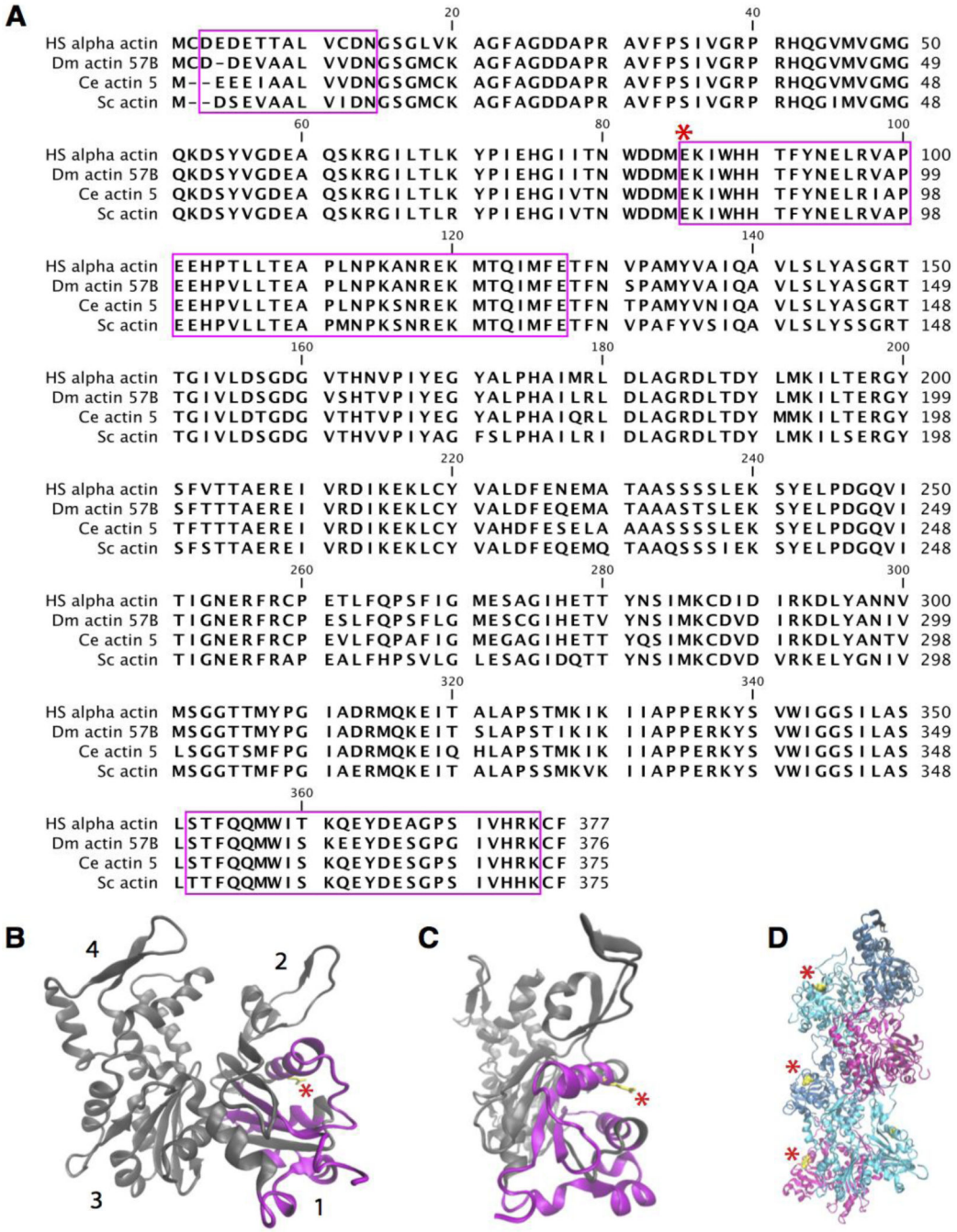

Fig. 3.

Glutamate 84 (E84) is a highly conserved residue and a part of the binding site for the CH domain superfamily. (A) Alignment of *Drosophila* (Dm) Actin 57B with homologs from *Homo sapiens (*Hs*), Caenorhabditis elegans (*Ce*) and Saccharomyces cerevisiae* (Sc). E84 (asterisk) is highly conserved from yeast to humans. Domains involved in binding members of the CH domain superfamily are indicated in magenta. (B-C) Crystal structure of the actin monomer is shown. The actin subdomains are denoted by numbers (1-4). E84 is highlighted in yellow and marked by an asterisk. The residues implicated in binding to members of the

CH domain superfamily are highlighted in magenta. (D) Crystal structure of F-actin consisting of six differentially colored actin monomers. E84 localizes to the outside surface of the filament and is highlighted in yellow and marked by an asterisk.

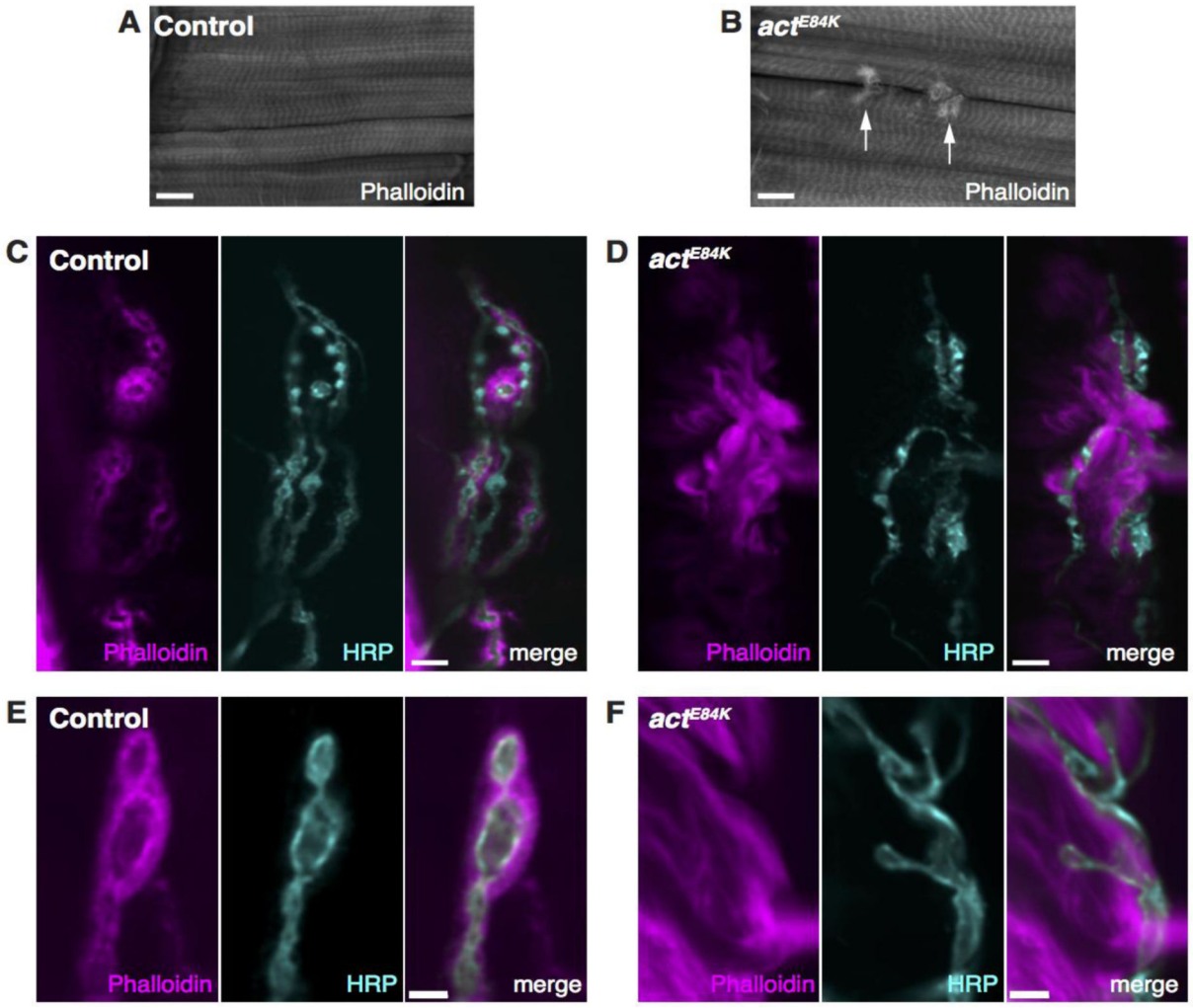

Fig. 4.

The postsynaptic actin cytoskeleton is impaired in *act*^{E84K} mutants. (A) Normal sarcomere structure observed in control animals revealed by phalloidin staining. (B) Sacromere structure is preserved in *act*^{E84K}. However, abnormal actin swirls are found that concentrate around the synaptic arbors of the NMJ (arrows). Scale bar in A and B, 20 μm. (C) Phalloidin and anti-HRP staining reveals the normal actin halo surrounding synaptic boutons at control NMJs. (D) The actin halo seen at control NMJs is disrupted in *act*^{E84K}. Instead, actin forms filamentous swirls that surround boutons. Scale bar in C and D, 10 μm. (E) A high magnification image of the postsynaptic actin cytoskeleton at a control NMJ is shown. (F) The normal halo pattern of actin organization shown in control is lost in *act*^{E84K} mutants, and wisps of actin filaments are observed instead. Scale bar in E and F, 2 μm.

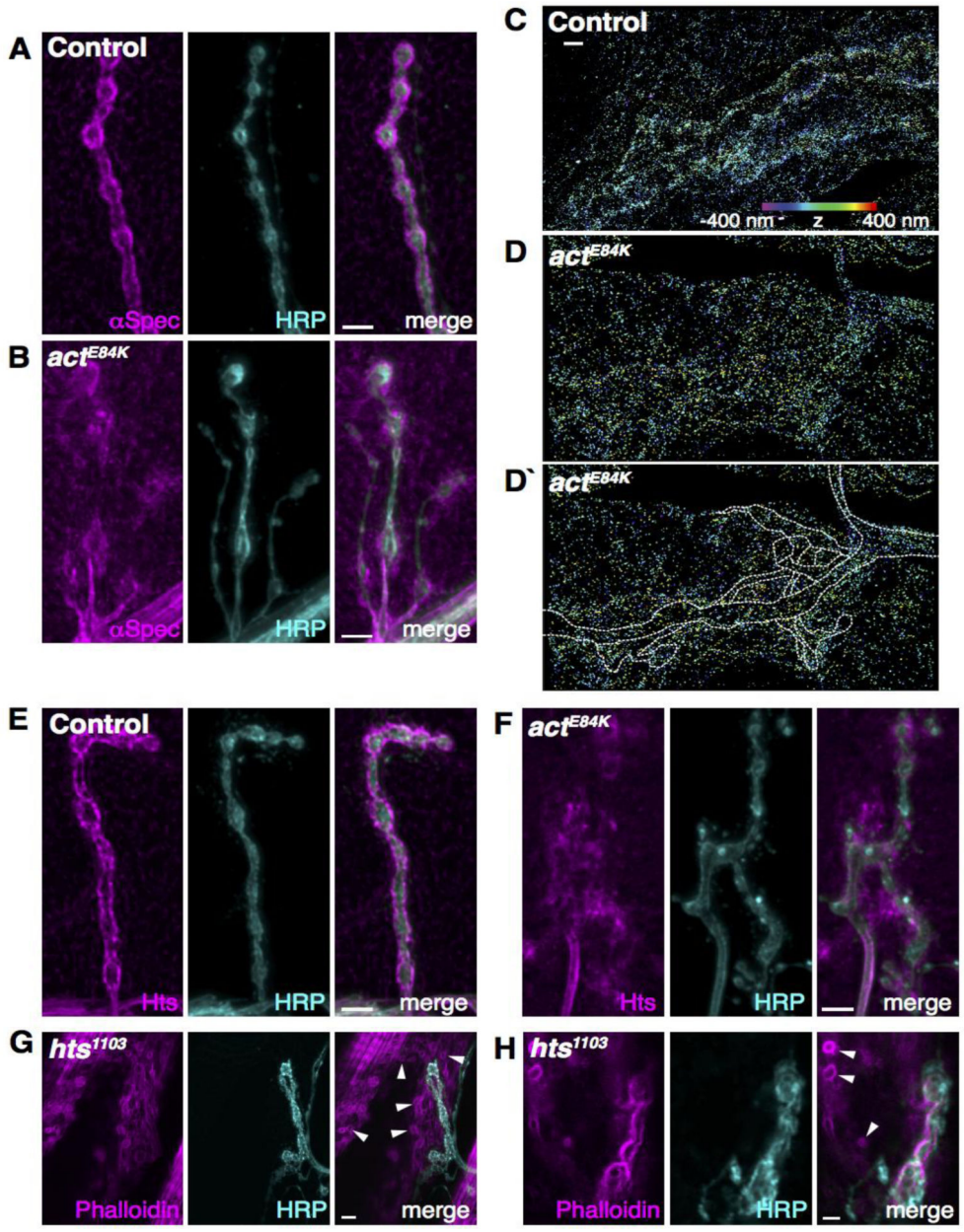

Fig. 5.

The postsynaptic spectrin network is disrupted in *act*^{E84K} mutants. (A, B) The normal localization of α-spectrin surrounding control boutons (A) is disrupted in *act*^{E84K} (B). Scale bar, 5μm. (C, D, D`) High-resolution three-dimensional STORM imaging reveals mislocalization of α-spectrin at the NMJ of *act*^{E84K} animals. Spectrin is normally clustered tightly around presynaptic boutons in control animals (C), but is diffuse and disorganized in *act*^{E84K} (D). An outline of the NMJ and axon (based on separate HRP staining) is shown for clarification (D`). Z positions in all STORM images are indicated by color, from −400 nm (violet) to 400 nm (red). Scale bar, 2 μm. (E, F) Adducin (Hts) is mislocalized in *act*^{E84K} (F) compared to control (E). Scale bar, 5μm. (G, H) The postsynaptic actin cytoskeletal organization is disrupted in *hts*^{1103} mutants, with the formation of actin rings (subset marked

by arrowheads) that are absent in cotnrols (compare to Fig. 4C). Scale bar, 5 μm in G and 2 μm in H.

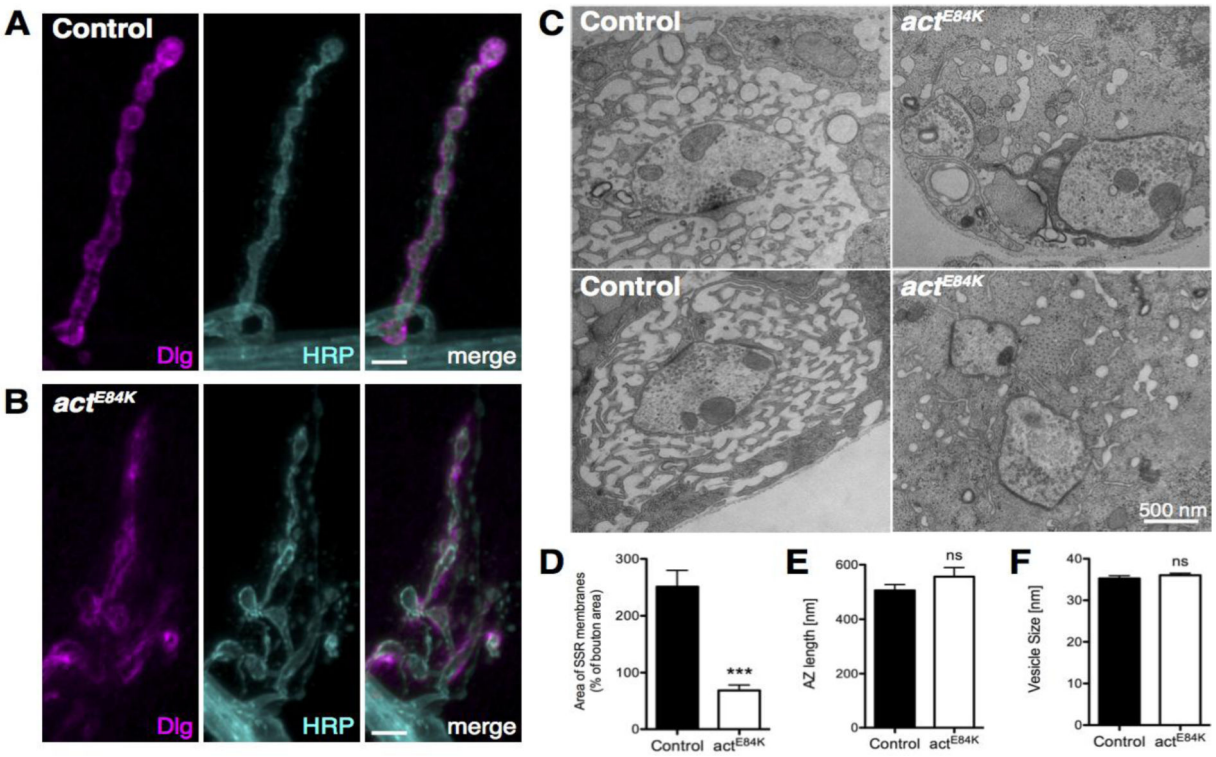

Fig. 6.

Localization of DLG and formation of the subsynaptic reticulum (SSR) is disrupted in *act*^{E84K}. (A, B) DLG localizes to the SSR in control animals (A), but is severely mislocalized in *act*^{E84K} mutants (B). Scale bar, 5 μm. (C) Ultrastructural EM analysis shows severe disruption of the SSR in *act*^{E84K} mutants compared to control. Muscle myofibrils can be observed to directly abut presynaptic membrane (arrowhead) upon loss of SSR membrane folds in *act*^{E84K}. Scale bar, 500 nm. (D) SSR area is severely reduced in *act*^{E84K} mutants (N=21 boutons from 3 larvae) compared to control (N=39 boutons from 5 larvae). (E) AZ length is not altered in *act*^{E84K} mutants (N= 31) compared to control (N=58). (F) Synaptic vesicle diameter is not altered in *act*^{E84K} mutants (N= 80) compared to control (N=80). Mean and SEM are indicated.

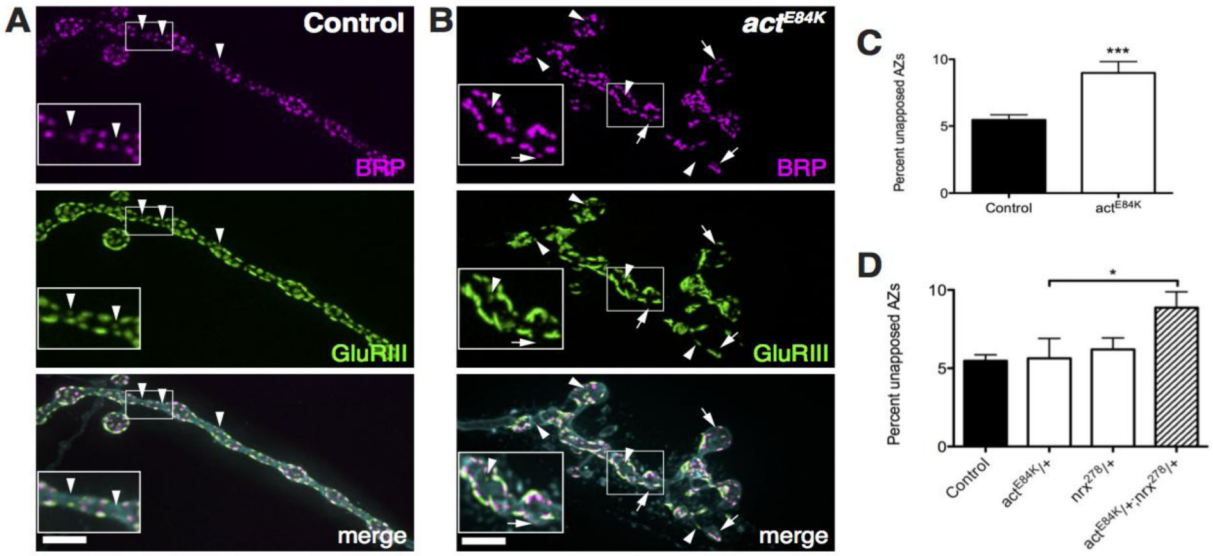

Fig. 7.

AZ and postsynaptic glutamate receptor fields are altered in *act*^{E84K} mutants. (A, B) Proper alignment of BRP and GluRIII clusters is disrupted in *act*^{E84K} mutants (B) compared to control (A). Unapposed GluRIII clusters (arrowheads) and BRP puncta (arrows) are highlighted. Insets show high magnification images of the boxed regions. Scale bar, 5 μm. (C) The fraction of unapposed AZs, either with GluRIII clusters or Brp puncta alone, is significantly larger in *act*^{E84K} mutants compared to control. (D) The number of unapposed AZs is increased in *act*^{E84K} and *nrx*^{278} double heterozygotes compared to control or single heterozygotes. Mean and SEM are indicated.

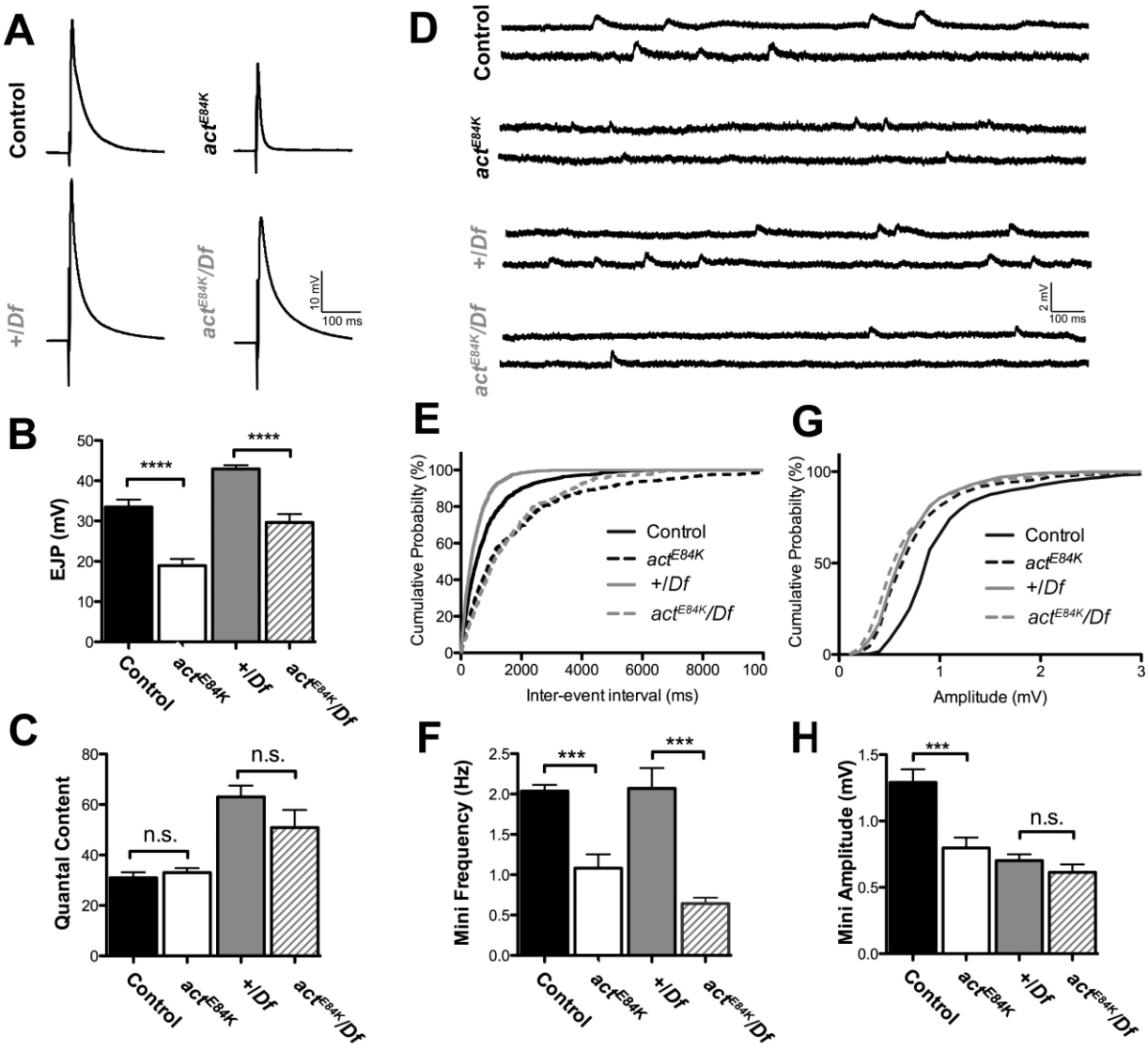

Fig. 8.

Synaptic transmission defects are observed in act^{E84K} and $act^{E84K}/Df(2R)Exel7166$ mutants. (A) Representative traces of evoked transmitter release in 1 mM extracellular Ca^{+2} are shown for control, act^{E84K}, $+/Df(2R)Exel7166$ and $act^{E84K}/Df(2R)Exel7166$ larvae. (B) EJP amplitude is significantly decreased in act^{E84K} and $act^{E84K}/Df(2R)Exel7166$ mutants compared to control [(control: 33.5 ± 1.8 mV, n=6; act^{E84K}: 18.9 ± 1.7 mV, n=7; $p \leq 0.0001$) and ($+/Df(2R)Exel7166$: 42.9 ± 0.9 mV, n=9; $act^{E84K}/Df(2R)Exel7166$: 29.6 ± 2.1 mV, n=6; $p \leq 0.0001$)]. (C) Quantal content is unchanged in act^{E84K} and $act^{E84K}/Df(2R)Exel7166$ mutants compared to control [(control: 31.0 ± 2.2, n=6; act^{E84K}: 33.1 ± 1.8, n=7; p=0.4667) and ($+/Df(2R)Exel7166$: 63.0 ± 4.5 mV, n=9; $act^{E84K}/Df(2R)Exel7166$: 50.9 ± 7.1 mV, n=6; p=0.1505]. (D) Representative traces of spontaneous mini release for each genotype. (E) Cumulative probability plot of inter-event intervals (ms) between mini events recorded from each genotype. (F) Average mini frequency is significantly decreased in act^{E84K} and $act^{E84K}/Df(2R)Exel7166$ mutants compared to control [(control: 2.0 ± 0.1 Hz, n=10; act^{E84K}: 1.1 ± 0.2 Hz, n=11; p=0.001) and ($+/Df(2R)Exel7166$: 2.1 0.2 Hz, n=10;

act^{E84K}/*Df(2R)Exel7166*: 0.6 ± 0.1 Hz, n=8.; *p*=0.0002)]. (G) Cumulative probability plot of individual mini amplitudes recorded from each genotype. (H) Average mini amplitude is reduced in *act*^{E84K} compared to control (control: 1.3 ± 0.1 mV, n=6; *act*^{E84K}: 0.8 ± 0.1 mV, n=11; *p*=0.001). Average mini amplitude is unchanged in +/*Df(2R)Exel7166* and *act*^{E84K}/*Df(2R)Exel7166* (+/ *Df(2R)Exel7166*: 0.7 ± 0.1 mV, n=10; *act*^{E84K}/*Df(2R)Exel7166*: 0.6 ± 0.1 mV, n=8; *p*=0.2693). Mini amplitudes are reduced in both +/*Df(2R)Exel7166* and *act*^{E84K}/*Df(2R)Exel7166* compared to control +/+ larvae ($p \leq 0.0001$ for both lines compared to control). In all figure labels, "+" = control chromosome and "*Df*" = *Df(2R)Exel7166*. Error bars represent SEM.